Neuron, Volume *95*

Supplemental Information

Neuronal Depolarization Drives Increased Dopamine Synaptic Vesicle Loading via VGLUT

Jenny I. Aguilar, Matthew Dunn, Susana Mingote, Caline S. Karam, Zachary J. Farino, Mark S. Sonders, Se Joon Choi, Anna Grygoruk, Yuchao Zhang, Carolina Cela, Ben Jiwon Choi, Jorge Flores, Robin J. Freyberg, Brian D. McCabe, Eugene V. Mosharov, David E. Krantz, Jonathan A. Javitch, David Sulzer, Dalibor Sames, Stephen Rayport, and Zachary Freyberg

Figure S1

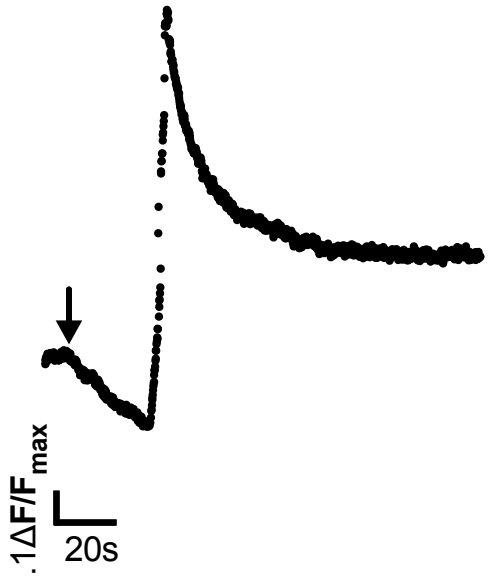

Figure S1: Related to Figure 1. KCl stimulation by pressure ejection causes rapid SV hyperacidification. Pressure ejection of KCl (10 s, arrow) onto an *ex vivo* whole fly brain preparation selectively expressing dVMAT-pHluorin in DA nerve terminals [*TH-GAL4, UAS-dVMAT-pHluorin*] caused an acute, rapid decrease in dVMAT-pHluorin fluorescence indicating SV hyperacidification. This effect preceded the expected brightening produced by vesicular exocytosis. The trace shows single-plane fluorescence intensity recorded at 100 ms intervals, integrated over the MB-MV1 region and normalized to initial values. Results are representative of n>3 independent experiments.

Figure S2

A

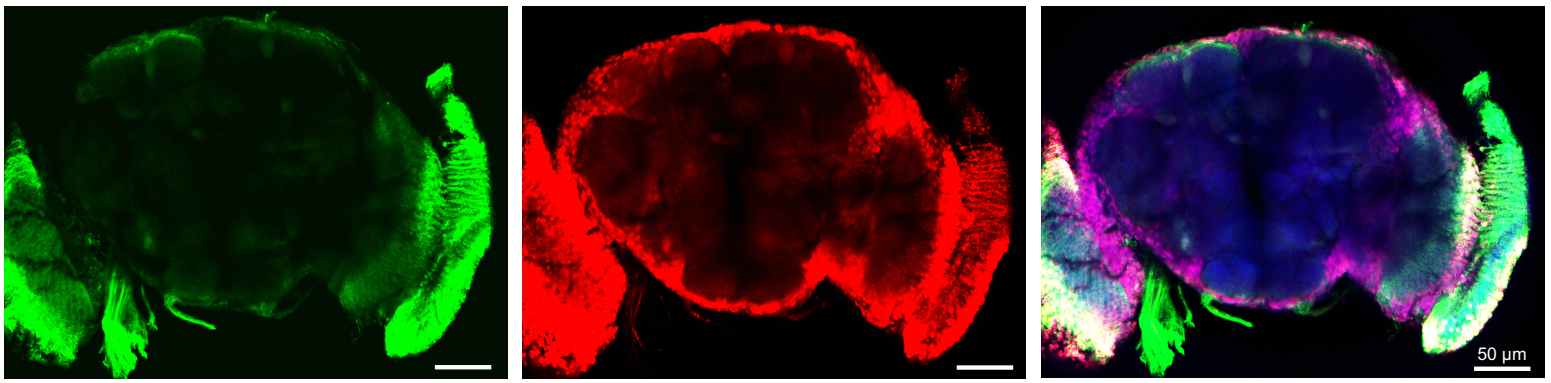

TH-GAL4>CD8-GFP VGLUT-LexA>mCherry Composite

B

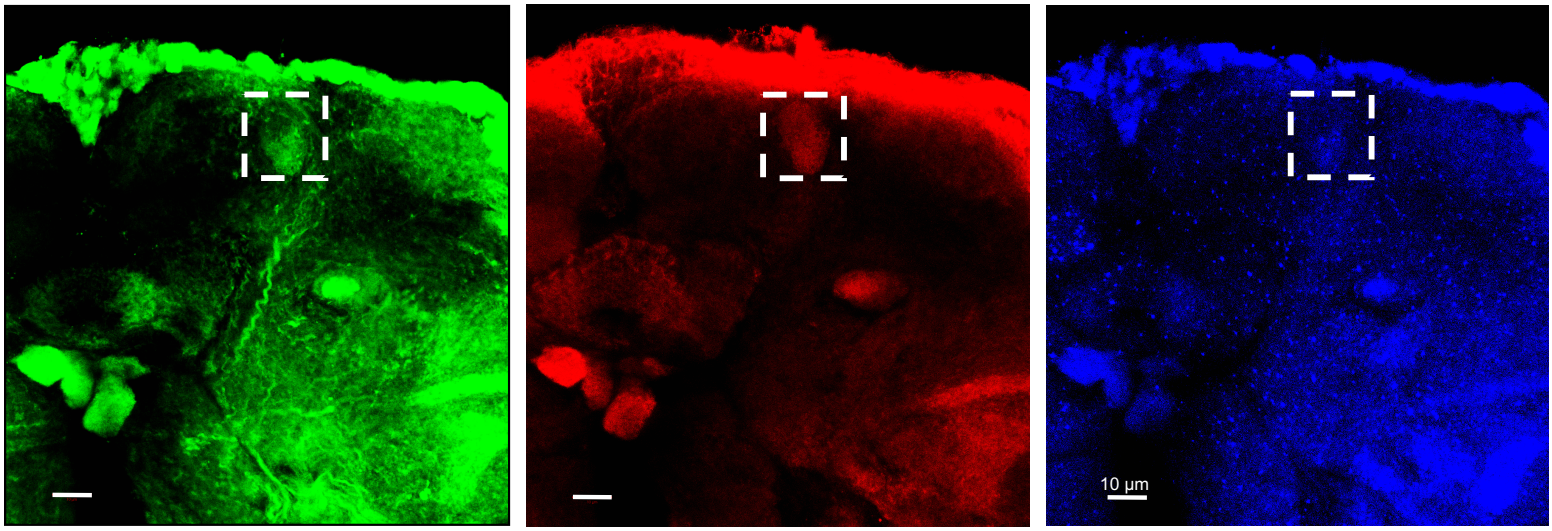

TH-GAL4>CD8-GFP VGLUT-LexA>mCherry nc82

Figure S2: Related to Figure 4. An overview of dVGLUT localization in a subpopulation of DA neurons in adult fly brain. Fluorescent tags were co-expressed by dVGLUT-LexA (mCherry) and TH-GAL4 (mCD8::GFP) enhancer-driven expression drivers. **(A)** Lower magnification overview images of the separate TH-GAL4-driven mCD8::GFP and dVGLUT-LexA-driven mCherry channels used to construct the merged composite image displayed in Figure 4A; a lower magnification of the overall composite image from Figure 4A is also shown (50 µm scale bar; false color). Each respective image represents a projected z-series. **(B)** Zoomed-out overview images of the TH-GAL4-driven mCD8::GFP, dVGLUT-LexA-driven mCherry and nc82 labeling featured in Figure 4B (MB-MV1 region boxed in white; 10 µm scale bar; false color). Each respective image represents a projected z-series. Fly strains used: *VGLUT-LexA/LexOP-6x mCherry;TH-GAL4/UAS-mCD8::GFP*. Data is representative of n>3 experiments.

Figure S3

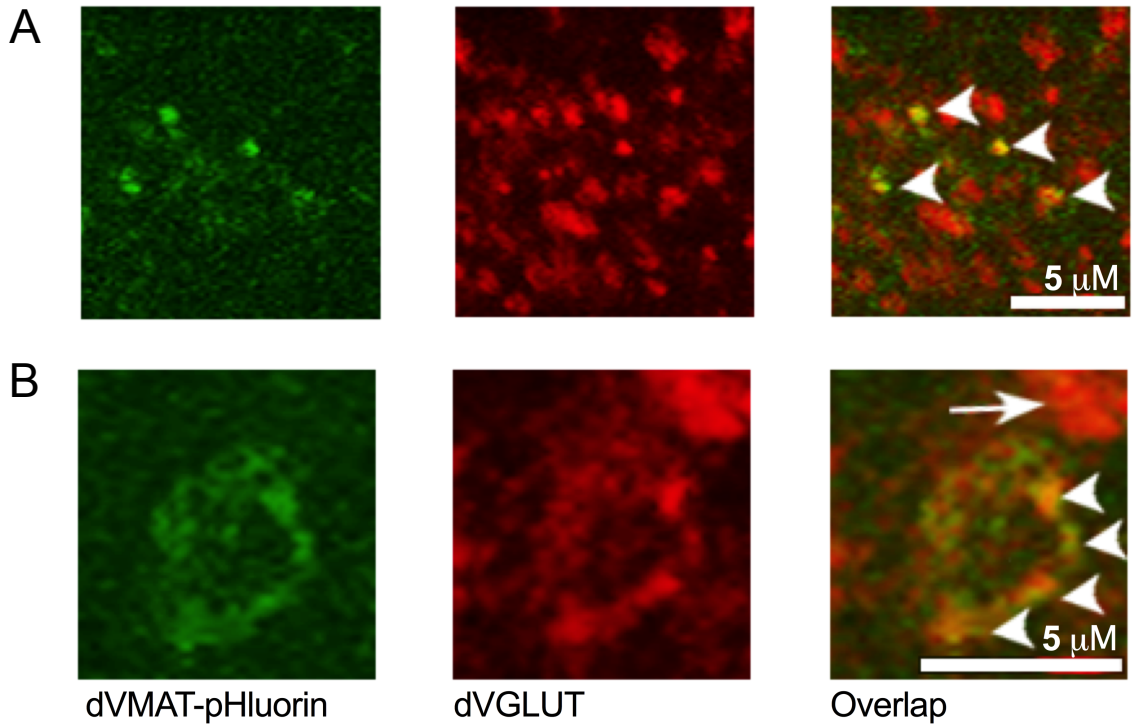

Figure S3: Related to Figure 4. A subpopulation of endogenous dVGLUT localizes to DA neurons in adult fly brain. To determine whether dVGLUT is present in presynaptic DA neurons, we co-labeled adult fly brains expressing TH-driven dVMAT-pHluorin [*TH-GAL4, UAS-dVMAT-pHluorin*] with antibodies to GFP (which also recognize pHluorin to identify DA neurons; in green) and to dVGLUT (in red), respectively. **(A)** Though endogenous dVGLUT labeling was detected throughout most of the brain neuropil, there was clear overlap between dVGLUT and dVMAT-pHluorin signals in DA nerve terminals as indicated in the merged image (yellow; arrowheads). **(B)** dVGLUT and dVMAT-pHluorin also co-localized in discrete varicosities within DA neuronal cell bodies (yellow; arrowheads); a cell body labeled only with dVGLUT is shown for comparison (in red; arrow). Results are representative of n>3 independent experiments.

Figure S4

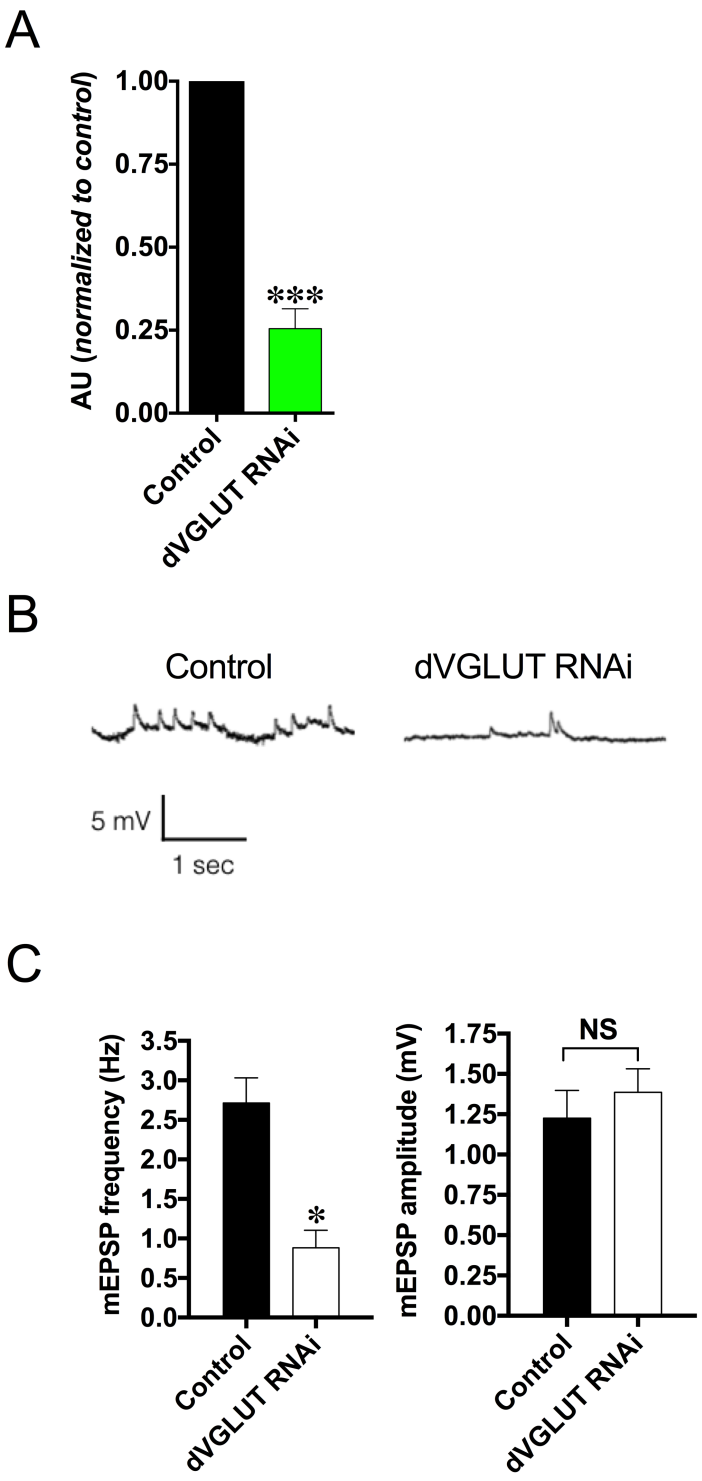

Figure S4: Related to Figure 5. Expression of dVGLUT RNAi in motor neurons inhibits the frequency of mEPSPs. (A) dVGLUT RNAi significantly reduced dVGLUT mRNA expression to 25.5±5.0% of the levels in GFP RNAi controls (n=3; p=0.0002). **(B)** Representative traces of miniature excitatory post-synaptic potential (mEPSP) recordings in flies expressing dVGLUT RNAi in larval motor neurons compared to wildtype controls. **(C)** Quantification of mEPSP frequency and amplitude revealed that presynaptic dVGLUT RNAi expression reduced the frequency ($p<0.01$) but not amplitude ($p>0.05$) of mEPSPs relative to the control. Fly strains: wildtype control [CantonS], dVGLUT RNAi [*OK6-GAL4/+; D42-GAL4/UAS-dVglut-RNAi*^{HMS}]. Intracellular recordings were used from muscle 6, segment A3 or A4. Results are representative of n=5 independent experiments for each respective condition. Error bars indicate SEM; *=$p<0.05$, **=$p<0.01$, ***=$p<0.001$.

Figure S5

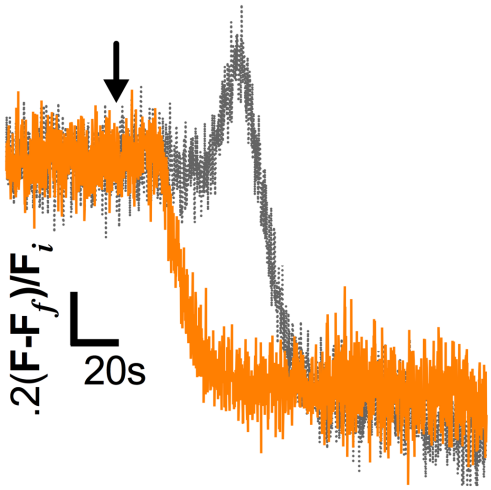

Figure S5: Related to Figure 5. Acute inhibition of dVGLUT inhibits depolarization-induced increases in SV loading. Acute dVGLUT inhibition by Rose Bengal (RB) pre-treatment attenuated depolarization-induced increases in DA vesicle loading in presynaptic DA nerve terminals (orange trace; 0.9±0.4% increase; n=4) compared to non-pretreated controls (black trace; 21.5±3.4% increase; n=4). The change in single-plane fluorescence ($F-F_f$) was normalized to baseline fluorescence after steady-state loading with FFN206 (F_i) and shown in the respective averaged FFN206 imaging traces. There was no significant difference in the rate of destaining in the RB pre-treated group ($t_{1/2}$=7.0±1.4 s; n=4) compared to non-RB pre-treated controls ($t_{1/2}$=5.2±0.9 s, n=4; p=0.005) as fit to a monoexponential decay (p>0.05). All fluorescent traces displayed a change in single-plane fluorescence intensity measured in ~250 ms intervals, integrated over the MB-MV1 region, corrected for background fluorescence, and normalized to initial values. A ~60 s baseline was recorded prior to KCl application (indicated by arrow). The KCl comparison group was also used in Figure 6. Error bars represent SEM. Fly strain: *dVMAT^{P1}; TH-GAL4, UAS-dVMAT*.

Figure S6

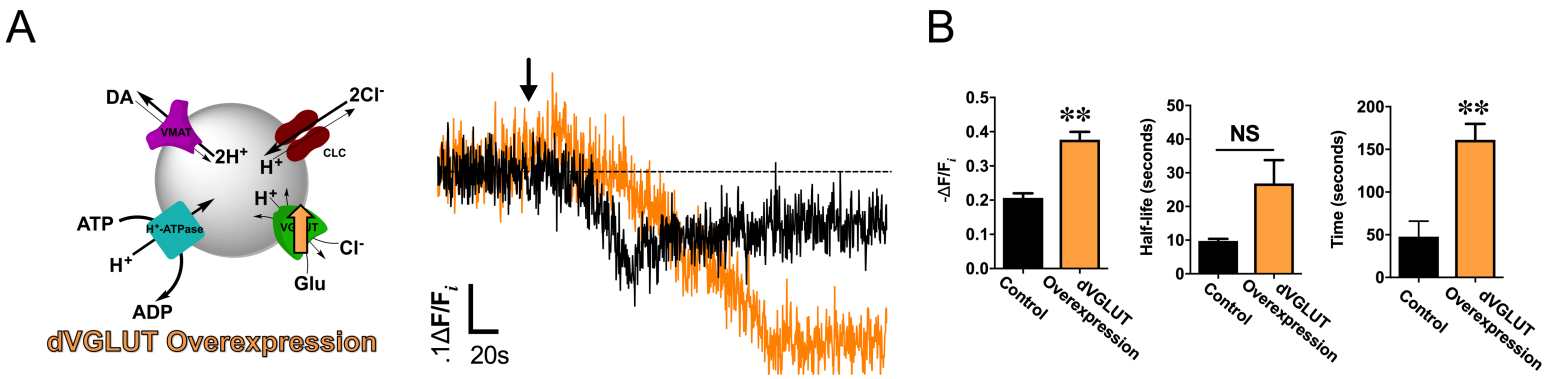

Figure S6: Related to Figure 5. Increasing dVGLUT expression enhances depolarization-induced SV acidification. (A) Left Panel: dVGLUT was selectively overexpressed in TH(+) presynaptic DA terminals. **Right Panel:** Averaged dVMAT-pHluorin fluorescence traces measuring DA vesicle pH during KCl-induced depolarization (40 mM; indicated by arrow) in adult fly brains overexpressing dVGLUT (orange trace, n=5) compared to control brains (black trace, n=3). All traces display a change in single-plane fluorescence intensity measured in ~250 ms intervals, integrated over the MB-MV1 region, corrected for background fluorescence, and normalized to initial values. **(B)** Enhancing dVGLUT expression in DA terminals significantly increased both the magnitude of SV acidification compared to baseline (n=3, p=0.002), and the absolute time to reach maximal vesicle acidification (p=0.005) relative to the control (n=5; p=0.005) during depolarization. dVGLUT overexpression did not significantly alter the half-life to reach maximal acidification compared to the control (p>0.05). Error bars represent SEM. Fly strains include: Control [*TeTxLC; TH-GAL4/+*]; dVGLUT overexpressed [*TeTxLC; TH-GAL4/UAS-dVGLUT*].

Figure S7

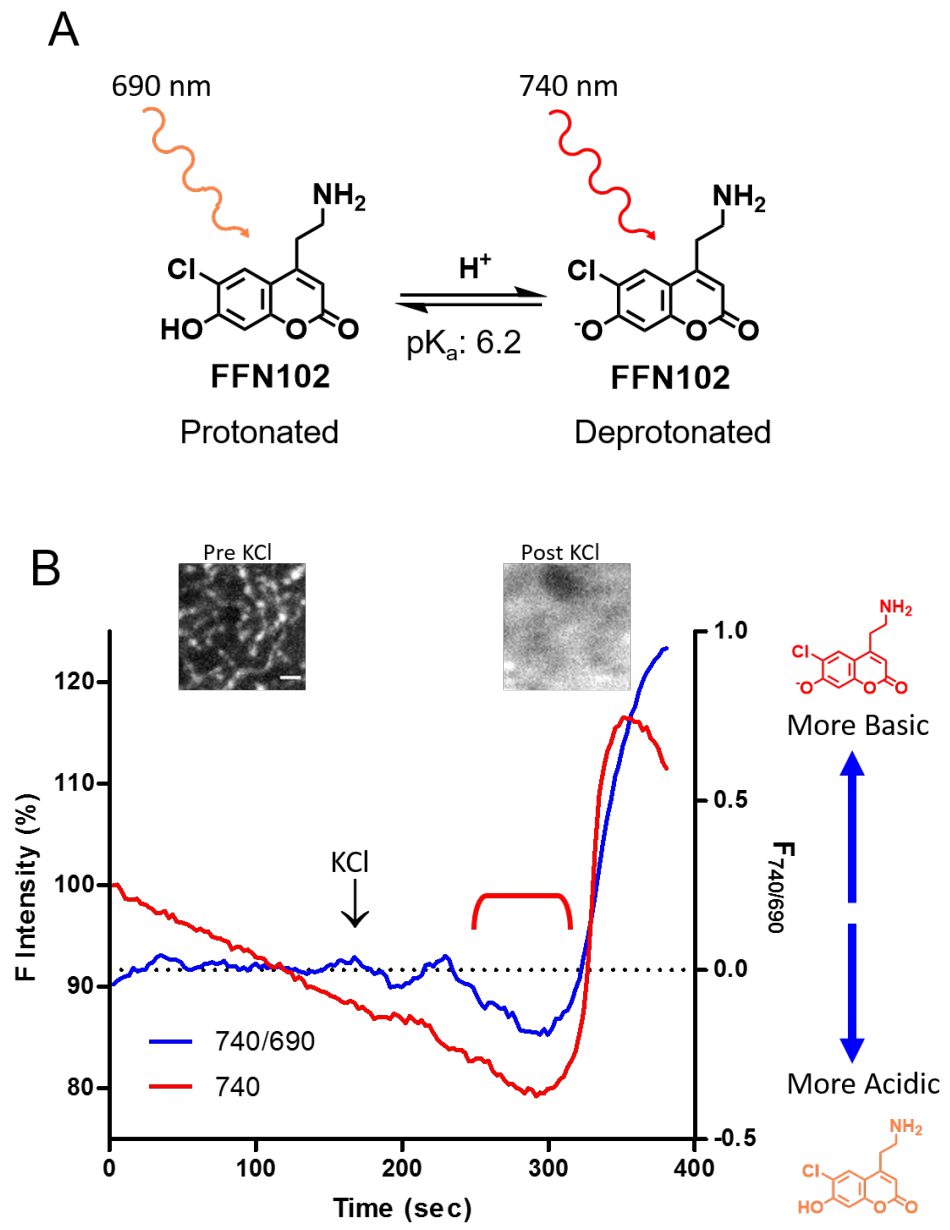

Figure S7: Related to Figure 7. Measuring relative changes in DA vesicular pH using ratiometric FFN102 fluorescence. (A) Schematic describing the equilibrium between protonated and deprotonated of FFN102. The 2-photon excitation maximum for protonated FFN102 is 690 nm and 740 nm for deprotonated FFN102. Relative concentrations of each species are measured in real time by calculating the ratio of fluorescence generated from each wavelength using the interlaced scanning of two lasers, permitting determination of the relative pH changes occurring within FFN102-labeled nerve terminals. **(B)** The ratio between FFN102 fluorescence emission (F_{740}/F_{690}) was simultaneously measured over a 6 min time-course in the presence of KCl stimulation (40 mM; applied at 150 s, arrow). Shown is a representative trace from a wildtype C57Bl6/J mouse acute medioventral striatal slice that includes the final normalized ratio (blue curve) and the change in single channel fluorescence in deprotonated FFN102 (740 nm, red curve). A large increase in fluorescence at 740 nm (~t=300 s) represents exocytic fusion and release of FFN102 release from the acidic SVs to the neutral extracellular space. FFN release was evident from the change in the FFN102 staining pattern between pre- and post-KCl images (**Inset**, scale bar = 2 μm). This vesicular FFN102 release was also observed in the change in F_{740}/F_{690} ratio between the deprotonated and protonated FFN102. We also observed a significant increase in KCl-induced vesicular acidification prior to vesicular fusion (indicated by red brackets; see Figure 7).

Figure S8

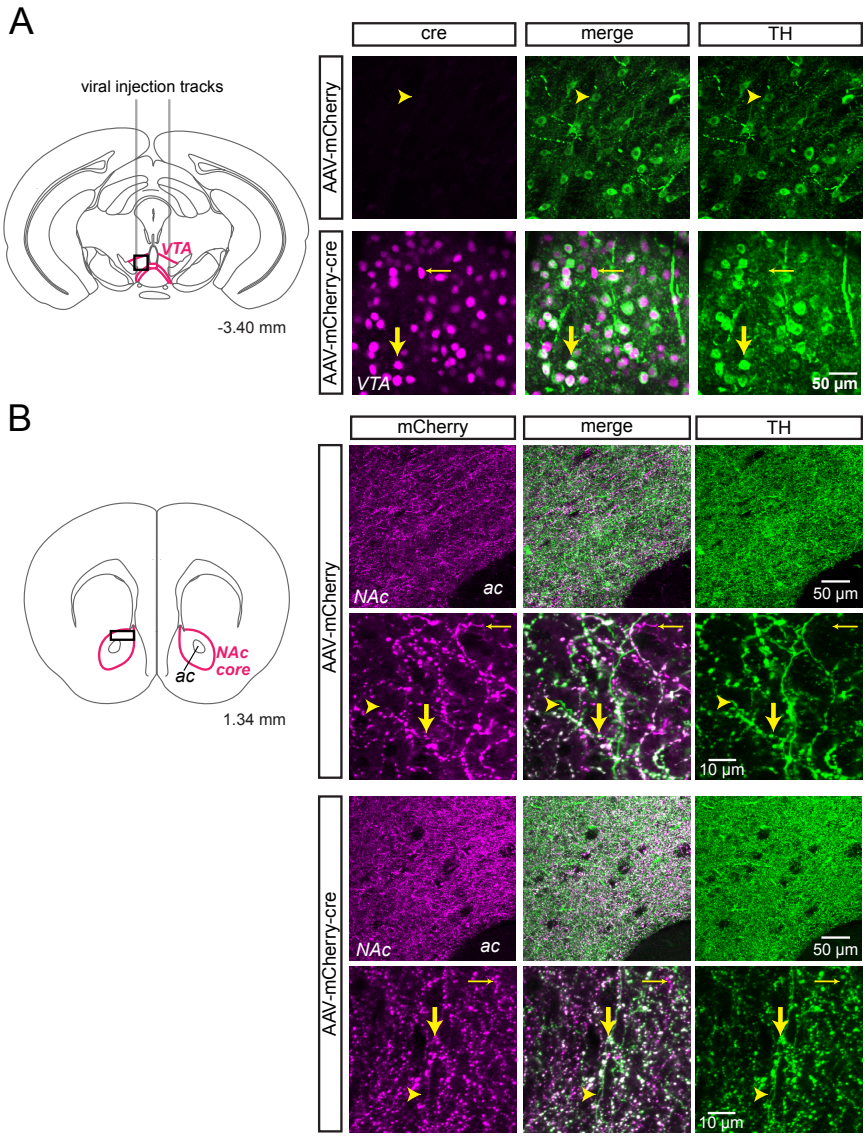
A
viral injection tracks
VTA
-3.40 mm
cre
merge
TH
AAV-mCherry
AAV-mCherry-cre
VTA
50 µm
B
NAc
core
ac
1.34 mm
mCherry
merge
TH
AAV-mCherry
AAV-mCherry-cre
NAc
ac
50 µm
10 µm

Figure S8: Related to Figure 7. Expression of *cre* or mCherry in VGLUT2$^{flox/flox}$ mice following VTA viral injection. (A) Schematic on the left shows the coronal brain slice through the VTA (outlined in magenta) used for immunostaining. The grey bars in the slice show the viral injection tracks and the black square around the injection site outlines the site of image acquisition. The photomicrographs on the right show the co-localization of *cre*-immunoreactive (ir-magenta) and tyrosine hydroxylase-ir (TH; green) signals in the VTA after injection of AAV-DJ EF1a-mCherry-cre (bottom row) as well as the absence of *cre*-ir following injection of AAV-DJ EF1a-mCherry (top row). The confocal z-projected images in the bottom row showed that the majority of TH(+) neurons expressed *cre*-ir (indicated by a thick yellow arrow and white staining in the merged bottom middle panel). This co-localization is indicated by a thick yellow arrow and white staining in the merged bottom middle panel. We also found a smaller portion of *cre*(+)/TH(-) cells (yellow arrowhead) and *cre*(-)/TH(+) cells (thin yellow arrow). **(B)** Schematic on the left shows the coronal brain slice through the NAc core (outlined in magenta) used for FFN102 recordings and subsequent immunostaining. The site of recordings and image acquisition in the NAc core is outlined by a black square. The photomicrographs on the right show the co-localization of mCherry (magenta) and TH (green) expression in the NAc after injection of AAV-DJ EF1a-mCherry-*cre* (bottom) or AAV-DJ EF1a-mCherry (top) virus. These confocal z-projected images showed almost complete co-localization of TH- and mCherry-ir in the NAc (as demonstrated by the thick yellow arrows), confirming that both types of AAVs successfully transduced VTA dopaminergic neurons that project to the NAc. The top rows for each respective viral injection consist of zoomed-out NAc images; bottom rows show zoomed-in images of the DA terminals. We also found a smaller portion of *cre*(+)/TH(-) terminals (yellow arrowhead) and *cre*(-)/TH(+) terminals (thin yellow arrow). Abbreviations: VTA, ventral tegmental area; NAc, nucleus accumbens; ac, anterior commissure. Images reflect results from n≥3 experiments.